Geophysics with applications to subsurface waste disposal: Case history

Ki Ha Lee
Ernest O. Lawrence Berkeley National Laboratory

Introduction

Recent development in geophysical methods allows us to accurately map the distribution of seismic velocity, density and electrical conductivity beneath the surface and between boreholes. These physical properties are dependent on porosity, fluid saturation, fluid conductivity, pressure, temperature, clay content, and in some circumstances, permeability. Hydrological parameters may be measured or inferred from drill hole experiments or directly from core samples. The point measurements in a drill hole are then interpolated to the interwell volume using either statistical properties of the local geology or reasonable estimates of the geological structure and lithology. More direct evidence is obtained from well tests, and interference tests between multiple wells, but these are ill posed inverse problems when it comes to defining the properties of the entire interwell volume. Furthermore such tests are impossible in the vadose zone. The interpolation of well data is often inaccurate or misleading and the central problem for all these studies is the lack of these fundamental parameters throughout the subsurface volume of interest.

Electrical and electromagnetic methods have been shown to be sensitive to the spatial and temporal variations of various hydrological parameters; porosity, fulid saturation, fluid type, pressure, and sometimes the temperature. These parameters are the keys to characterizing waste disposal sites and predicting the extent and eventual migration paths of subsurface contaminants including radioactive waste. Fluid flow and chemical transport in unsaturated fractured rocks have been the primary subject of research interests in the siting of radioactive waste repositories and remediation of contaminated sites. This paper provides an overview of some of the application of electrical and electromagnetic methods in understanding the subsurface hydrology. Furthermore, a non-invasive electromagnetic method is introduced for high-resolution mapping of electrical resistivity and water saturation at shallow (< 10m) depths.

Case studies

1) Box Canyon fractured basalt site

A conceptual model of the geometry and physics of water flow in a fractured basalt vadose zone was developed based on the results of lithological studies and series of ponded infiltration tests conducted at the Box Canyon (Faybishenko et al., 2000), Idaho. The site is located in the Eastern Snake River Plain near the Idaho National Engineering and Environmental Laboratory (INEEL) (Figure 1). The Box Canyon site is an environmentally clean analog site for contaminated sites at INEEL. Minimal soil cover and a nearby cliff face exposure (Figure 2) provide an excellent opportunity to study the relationships between the fracture pattern and the hydrologic response to the infiltration tests.

The Snake River Plain is primarily composed of fractured Quaternary basalt flow units, inter-layered with sedimentary deposits. Sedimentary interbeds may separate basalt flow units formed at widely separated times, and their thickness may range from a few centimeters to as much as 15 m. Basalt flows are typically highly fractured, and geophysical logging and coring results suggest that the total basalt thickness in this area may exceed 3 km (Knutson et al., 1993). In general, the upper two thirds of the basalt flow is characterized by small fracture spacing and thus has more fractures then the lower third. In some basalt flows, there is a region near the center of the basalt flow that contains highly fractured rock that does not display the columnar style of fracturing (Long and Wood, 1986). These subhorizontal central fracture zones are present in about 40% of basalt flows examined at Box Canyon (Figure 2). On the basis of the results of experiments on core samples by Knutson et el. (1990) the porosity of the basalt matrix ranges from 20 to 40%, and the geometric mean permeability is 2.24×10^{-15} m^2 (biased toward low permeability, greater than 10^{-12} m^2 from vesicular zones were excluded in this estimation). Over the course of 3 years (1995-1997), there were 38 vertical and inclined boreholes drilled (diameters of 10 – 15 cm) and logged (natural gamma and caliper measurements, video recording, borehole scanning, and core description). These boreholes were used to study the types of fractures, the depth of soil infilling the fractures, the occurrence of vesicular zones, and the locations of fracture and rubble zones (Faybishenko et al., 1998a, 1998b). Figure 3 shows a 3D view of the borehole layout and the lithology obtained from the core.

On the bases of parameter estimations, results of borehole logging studies and the geometric conceptual model of the fracture pattern, the scale of the infiltration tests was determined and a series of tests (one in 1996 and four in 1997) has been conducted. The objective of the tests was to simulate episodic surface flooding events that occur during large rainstorms or snowmelt events. Tracer tests were also carried out by adding a slug of potassium bromide (KBr) solution to the water. Types of data collected during the tests include cumulative volume of water, evaporation rate, local infiltration rates, water pressure, tracer samples, moisture and its temporal changes, temperature, electrical resistivity and cross borehole ground penetrating radar (GPR) using the pulseEKKO 100 of Sensors & Software.

Since this review is focused on the use of electrical and electromagnetic methods in conjunction with the monitoring of moisture contents during and after the infiltration tests, we will first examine the result of a simple test using miniature electrical resistivity (ER) probes. Temporal variations occurred in all tests with decreases in resistivity (Figure 4a), which may be interpreted as an increase in tracer concentration. Nearly all the ER probes (96%) located near fractures or in the central fracture zone showed decrease in resistivity during the tests in 1997, indicating that the tracer eventually reached most fractures (Figure 4b).

Figure 5 shows the results of neutron logging in well R-3 corresponding to three, one in 1996 and two in 1997, infiltration events. A major increase in moisture content took place at a depth interval of 7 to 11 m at the end of the first test (1996), and it stayed unchanged throughout the rest of the tests. The moisture increase at this depth indicates a strong horizontal flow beneath and beyond the infiltration pond (notice R-3 is slanted). Along with the neutron logging cross borehole GPR surveys have been conducted between boreholes II4 and I4 before and during the test in 1996. These boreholes are

vertical and closer to the cliff than the R-3 well. Figure 6 shows the difference in radar pulse velocity, with the red indicating the decrease in velocity, or increase in moisture content. There were several local increases in moisture content, especially within the central fracture zone and the rubble zone. As is the case of neutron logging no significant changes in velocity were observed using GPR. Notice that the rubble zone with a major increase in moisture identified by the neutron logging is lower than that by GPR. This is because the rubble zone is dipping into the cliff.

2) Yucca Mountain

The US Department of Energy (DOE) has been evaluating the unsaturated zone (UZ) at Yucca Mountain, Nevada, as a potential repository site for high-level nuclear waste. The site is located about 120 km northwest of Las Vegas. It is remote and sparsely populated, and has low rates of infiltration (5mm/yr) and a thick (600-700m) UZ. A total of 60 deep boreholes have been drilled from the surface and an 8-km long tunnel, the Exploratory Studies Facility (ESF), was completed in 1996. The proposed repository would be located approximately 300m below the surface and about the same distance above from the water table. An overview of scientific investigation at Yucca Mountain is given by Bodvarsson et al. (1999).

The boreholes and ESF have yielded a large number of thermal, geological, hydrological, and geochemical data. As the first of the two large scale in situ heater tests, the Single Heater Test (SHT) was conducted starting from 1996 through early part of 1998 (Tsang, 1999). The SHT provided valuable insights in testing methods, data acquisition logistics, data interpretation, and modeling strategies. These results are very useful for the much larger scale and longer duration Drift Scale Test (DST) initiated in 1997. This paper highlights some of the results of modeling studies (Birkholzer and Tsang, 2000) of the early part of the 8-year-long DST heater test. The primary objective of the DST is to acquire a more in-depth understanding of the coupled thermal, mechanical, hydrological, and chemical processes likely to exist in the host rock of the potential geological repository.

Figure 7 shows a three-dimensional perspective of the DST, with heaters and instrument boreholes for measuring thermal, hydrological, mechanical, and chemical processes. The DST centers around the heated drift with a 47.5 m-long heated section. Heating is provided by nine canister heaters within the heated drift, and 50 wing heaters placed in 11.5 m-long horizontal boreholes that flank the north and south sides of the heated drift (Figure 8). Modeling of the thermal-hydrological processes in the DST was performed using the numerical simulator TOUGH2 (Pruess, 1987, 1991; Wu et al., 1996) for simulating coupled transport of water, water vapor, air, and heat in heterogeneous porous and fractured media. Figure 9 shows a close-up view of 2-D x-z cross section intersecting the heated drift, containing the five hydrology holes 57 through 61. Simulated temperature and saturation are compared with the actual measurements as the heating experiment is continued. In addition a tomogram of saturation change from the pre-heat ambient values derived from cross-hole GPR survey taken in January of 1999 is shown in Figure 10. The GPR tomogram along with periodic measurements of neutron logging data all indicate an expanding drying zone around the heated drift and the wing heaters with time, and wetting zones beyond the dry volume.

Electromagnetic impedance for near-surface application

Non-invasive sensing of the shallow subsurface is often required for detection and delineation of buried hazardous wastes, monitoring of the condition of clay containment caps, and a variety of other purposes. Electromagnetic methods have been shown to be effective in environmental site characterization, but there is a need for increased resolution for waste form characterization, verification, and monitoring activities. A window exists in the electromagnetic spectrum between GPR frequencies (30 MHz to 1 GHz) and induction technique frequencies (<100 kHz) that has not been utilized for these applications (Figure 11). Two considerations strongly suggest the use of frequencies in this band for such applications: 1) the induction response of many targets is small due to small size, and 2) a need to determine both the electrical conductivity and dielectric permittivity which is directly related moisture content. Modeling and physical parameter studies confirm that measurements at frequencies between 1 and 100 MHz can yield resolution of subsurface conductivity and permittivity. The term "high frequency" as used herein refers to this region of the radio spectrum.

As one of the promising technologies the electromagnetic impedance, the ratio of orthogonal horizontal electric to horizontal magnetic fields, method has been under development at the Lawrence Berkeley National Laboratory. The effective depth of investigation for surface impedance measurements depends on the frequency, and is commonly expressed in terms of the skin depth, the distance into the conductive half space at which the amplitude of the incoming wave has decreased to e^{-1} of its surface value. In order to achieve skin depths between 0.5 and 10 meters in material of resistivity between 1 and 100 ohm-m and relative permittivity between 1 and 30, frequencies between about 300 kHz and 100 MHz are required.

To emphasize the utility and the importance of high-frequency electromagnetic measurements for mapping subsurface distribution of moisture content, we take as example a clay cap model. Figure 12 presents a simple clay cap application, based on conditions at the US Department of Energy's Savannah River Site H-Area Basin, where the specific problem is the shrinkage-induced cracks in the clay cap as it dries. Measured resistivities are about 500 ohm-m (Persoff, et al., 1996). The relative permittivity calculated from an experimentally validated standard mixing law (Knoll, 1996) for a clay-air-water mixture ranges from 17 or greater for a healthy clay to 12 and less for one which is too dry for regulatory compliance. Thicknesses and expected permittivities are shown for all layers of the cap. The surface 'plane-wave' impedance, in ohms, calculated by taking the ratio of electric to magnetic fields, is plotted against frequency. As is apparent, the good and bad clay conditions manifest themselves in a 27% difference in amplitude at about 30 MHz. Adjusting only the layer resistivities within the ranges observed at the site, however, perturbs these curves by less than 5%. The same geometry with the observed resistivities and equal permittivities yields a nearly featureless spectrum. The change in impedance is caused solely by permittivity contrast, which cannot be detected by any conductivity-sensitive method. Variation of the clay water content yields little change in resistivity, since surface conduction dominates over saturation effects. A GPR survey did not result in clear images in tests done at a nearby

site composed of the same clays and soils. Clearly, quantitative knowledge of the layer permittivity is required to solve the problem.

To demonstrate the utility of the high-frequency impedance (HFI) method a prototype 0.1 to 30 MHz system was assembled over the past three years using off-the-shelf components including a magnetic dipole transmitter, electric and magnetic antennae. Three fiber-optic coupling systems were used to achieve the necessary isolation between source and receiver. Magnetic and electric field sensors are typically positioned at a height of about one meter. The prototype HFI system components are shown in Figure 13. Field tests were done in the relatively conductive (20 to 50 ohm-m) environment of the University of California's Richmond Field Station and a far more resistive ones (2,000 to 10,000 ohm-m) at the Point Reyes National Seashore and Donner Summit. Encouraging results were obtained at all the sites. Some of the results are summarized in this report.

Figure 14 shows observed and fitted data from the Richmond site. A DC resistivity sounding at this location shows a resistive, 0.4-m thick upper layer of about 200 ohm-m overlying a half space of about 40 ohm-m, which is in good agreement with the interpreted model. The permittivity is not well resolved due to the low resistivity. These data demonstrate that the high frequency measurements are accurate since they do include the independently determined layered resistivity structure. The permittivity values were unverified but appear reasonable for the test environment.

The presently available proof-of-concept equipment is not well suited for extensive field experimentation. A more mobile system is currently being assembled by repackaging the basic components and replacing a few of the more provisional ones with smaller, more rugged alternatives. A control module will house the computer, lock-in amplifiers, function generator, and the three fiber optical systems. The sensors and the transmitter system will be mounted on wheels using a rigid, non-conducting frame. A sketch of the contemplated cart is shown in Figure 15.

The repackaged system is envisioned in three modules, one each for the transmitter, the receiver, and the control functions, plus the cart. The transmitter module will contain the source antenna, an RF amplifier, a fiber-optic receiver, and a power supply. The receiver module will mount the two field sensors (electric and magnetic) and two fiber-optic transmitters; power requirements are minimal and should be handled by small batteries for each individual unit to maintain isolation. The control module will host the control computer, function generator, lock-in amplifiers, two fiber optic receivers, one fiber optic transmitter, and a power supply. In operation, the computer sets the function generator frequency (and perhaps amplitude); the output is supplied to the fiber optic transmitter for transmission to the transmitter module and to the lock-ins as a phase reference.

Acknowledgments

I thank Boris Faybishenko and Yvonne Tsang of LBNL for providing materials in completing the case history part of this review paper. This work was supported by the EMSP Program under the Assistant Secretary for Environmental Restoration and Waste Management, Office of Technology Development, of the U.S. Department of Energy under contract No. DE-AC03-76SF00098.

References

Birkholzer, J.T., and Tsang, Y.W., 2000, Modeling the thermal-hydrologic processes in a large-scale underground heater test in partially saturated fractured tuff, Water Resources Research, 36, 1431-1447.

Bodvarsson, G.S., Boyle, W., Patterson, R., and Williams, D., 1999, Overview of scientific investigations at Yucca Mountain – the potential repository for high-level nuclear waste, Jour. of Contaminant Hydrology, 38, 3-24.

Faybishenko, B., Doughty, C., Steiger, M., Long, J.C.S., Wood, T.R., Jacobson, J.S., Lore, J., and Zawislanski, P.T., 2000, Conceptual model of the geometry and physics of water flow in a fractured basalt vadose zone, Water Resources Res., 36, 3499-3520.

Faybishenko, B., Holland, P., Mesa, M., Burgess, D., Knutson, C., and Sisson, B., Lithological conditions at Box Canyon site: Results of drilling, core and open borehole measurements, 1995-1997 data report, Rept. LBNL-40182, E.O. Lawrence Berkeley Natl. Lab., Berkeley, Calif., Sept. 1998a.

Faybishenko, B., Salve, R., Zawislanski, P., Lee, K.H., Cook, P., Freifeld, B., Willaims, K., and Doughty, C., Ponded infiltration test at the Box Canyon site: Data report and preliminary analysis, Rept. LBNL-40183, E.O. Lawrence Berkeley Natl. Lab., Berkeley, Calif., Sept. 1998b.

Knoll, M.D., A petrophysical basis for ground penetrating radar and very early time electromagnetics: electrical properties of sand-clay mixtures: Ph.D. dissertation, Univ. Brit. Columbia, July 1996.

Knutson, C.F., Cox, D.O., Dooley, K.J., and Sisson, J.B., Characterization of low-permeability media using outcrop measurements, SPE Paper 26487 presented at 68th Annual Technical Conference and Exhibition, Soc. Pet. Eng., Tex., Oct. 3-6, 1993.

Long, P., and Wood, B., 1986, Structures, textures, and cooling histories of Columbia River basalt flows, Geol. Soc. Am. Bull., 97, 1144-1155.

Persoff, P., Moridis, G.J., James, A., and Frangos, W., Laboratory study of closure cap repair techniques, Rep. LBNL-39420, E.O. Lawrence Berkeley Natl. Lab., Berkeley, Calif., Dec. 1996.

Pruess, K., TOUGH user's guide, Rep. LBL-20700, Lawrence Berkeley Natl. Lab., Berkeley, Calif., 1987.

Pruess, K., TOUGH2 – A general purpose numerical simulator for multiphase fluid and heat flow, Rep. LBL-29400, UC-251, Lawrence Berkeley Natl., Lab., Berkeley, Calif., 1991.

Tsang, Y.W., 1999, A field study for understanding thermally driven coupled processes in partially saturated fractured welded tuff, Int. Jour. of Rock Mech. and Min. Sci., 37, 337-356.

Tsang, Y.W., and Birkholzer, J.T., 1999, Predictions and observations of the thermal – hydrological conditions in the Single Heater Test, Jour. of Contaminant Hydrology, 38, 385-425.

Wu, Y.S., Ahlers, C.F., Fraser, P., Simmons, A., and Pruess, K., Software qualification of selected TOUGH2 modules, Rep. LBNL-39490, Lawrence Berkeley Natl. Lab., Berkeley, Calif., 1996.

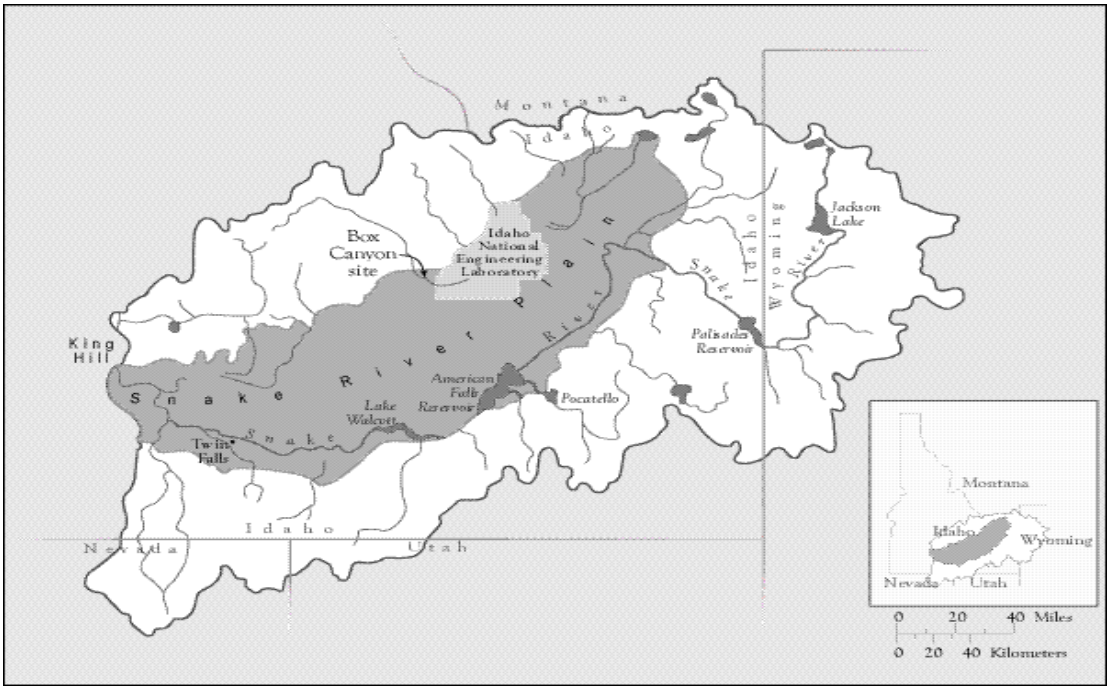

Figure 1. Map of the Eastern Snake River Plain and the location of the Box Canyon.

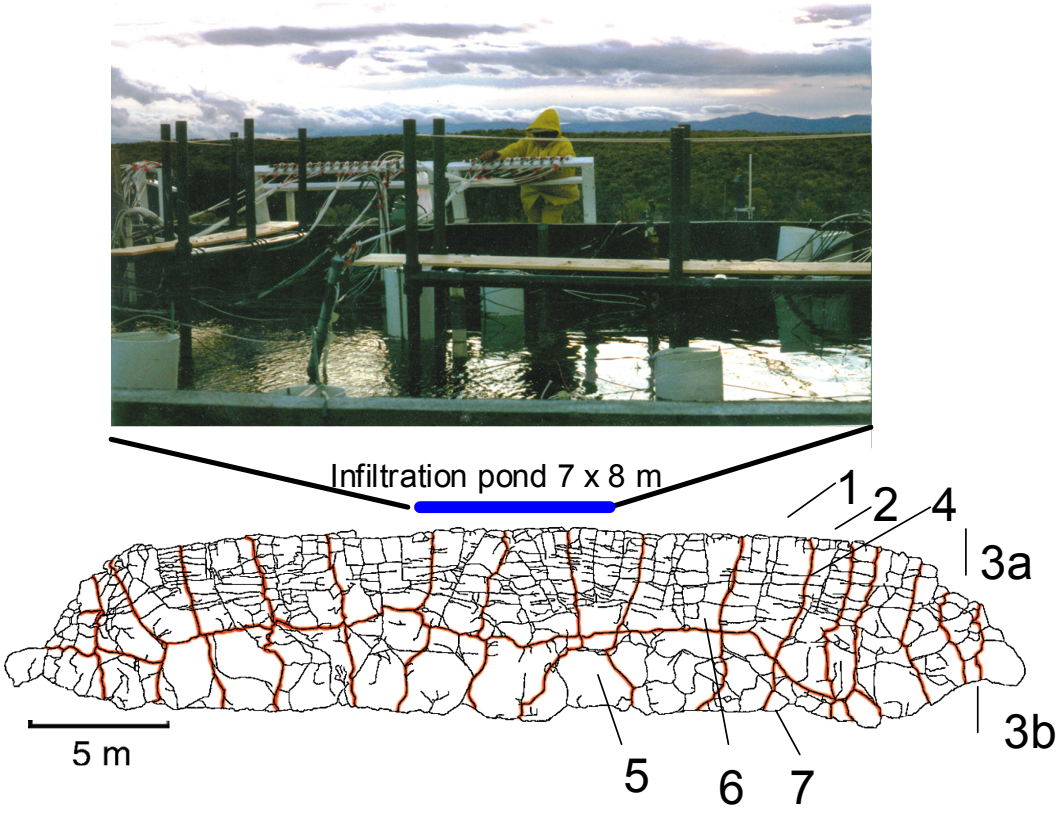

Figure 2. Box Canyon infiltration pond and a two-dimensional map of the fracture pattern at the vertical vasalt outcrop, showing the main functional geological components affecting water flow.

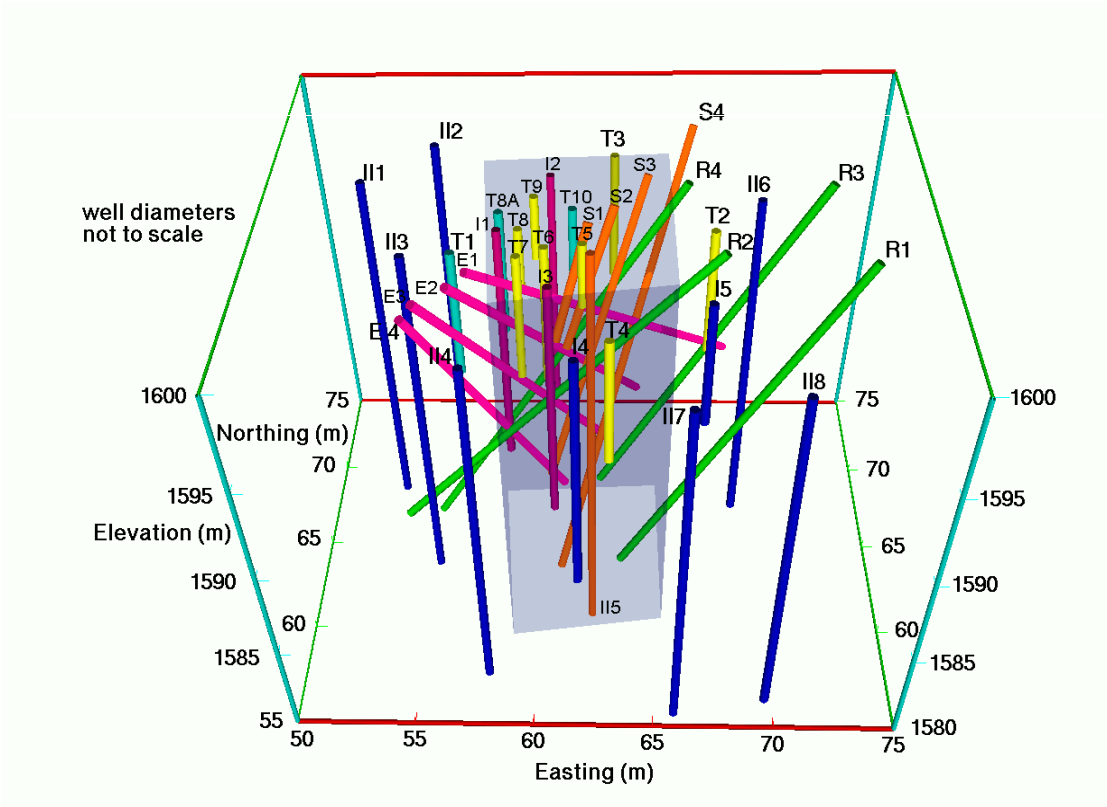

Figure 3. Perspective view of well layout at the Box Canyon.

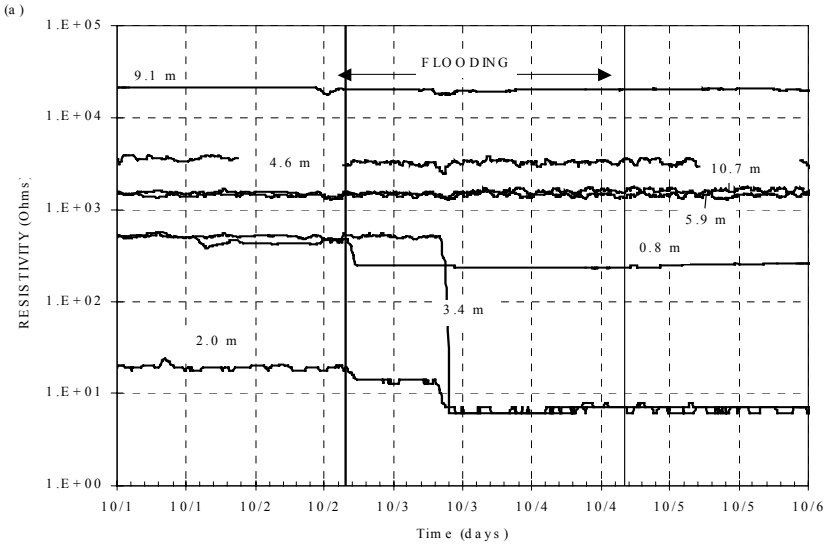

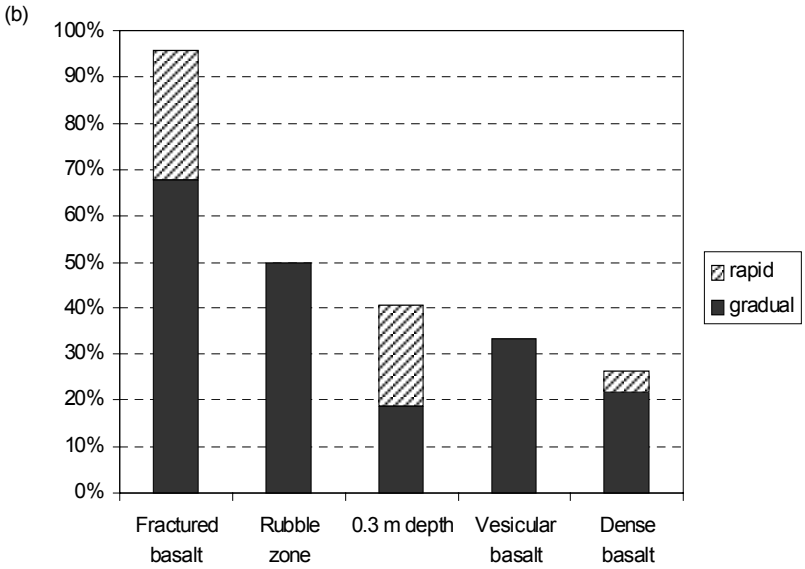

Figure 4. Results of ER probe measurements: (a) example of temporal ER response in well S-3, and (b) classification of all ER probe measurements.

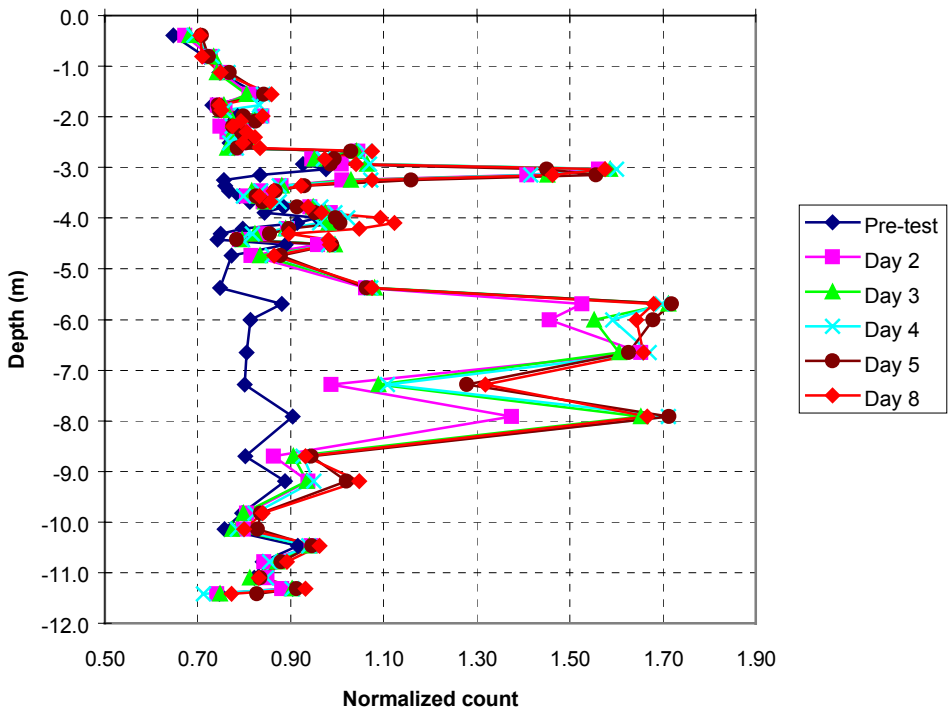

Figure 5. Normalized neutron probe count readings at well r-3 – 1996

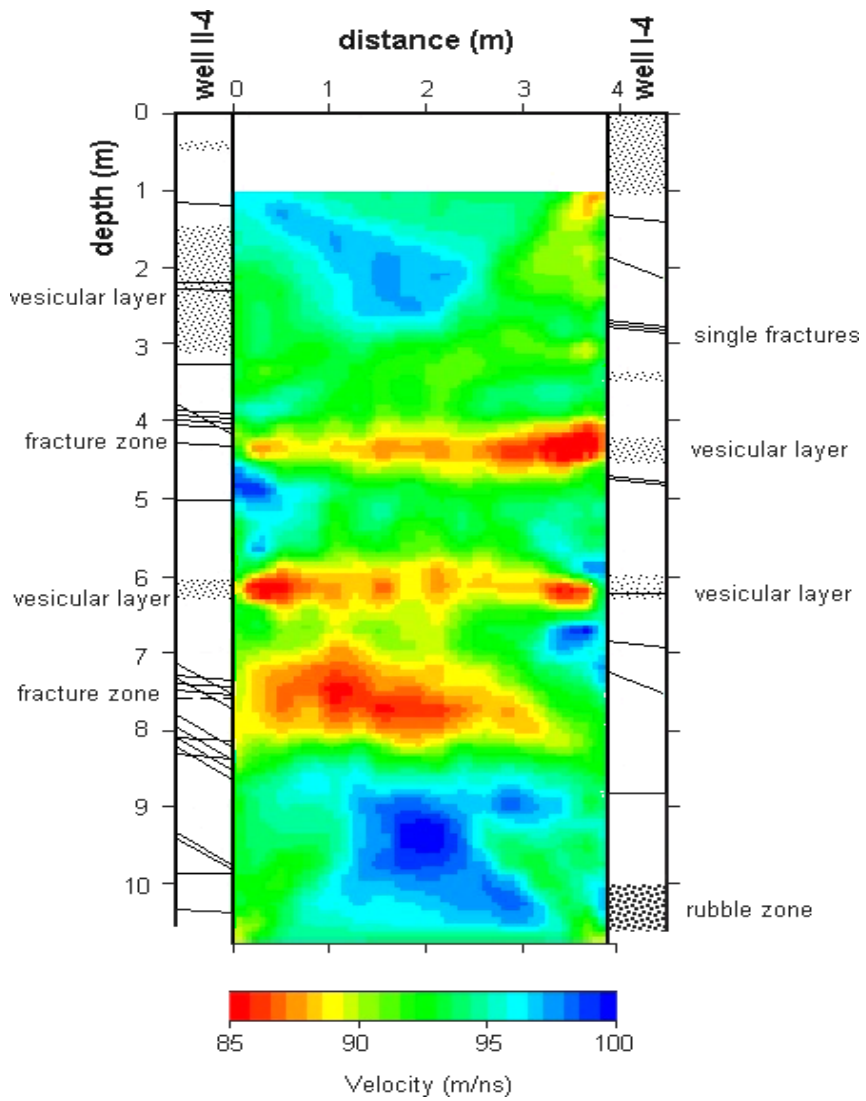

Figure 6. An electromagnetic wave velocity difference tomogram obtained from GPR surveys conducted prior to and during test 96-1.

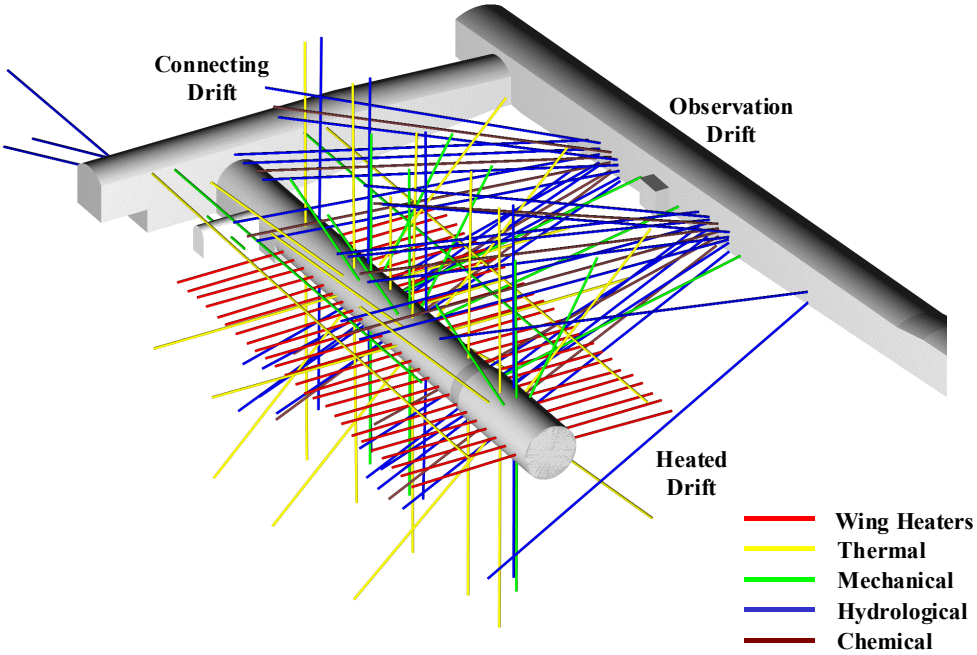

Figure 7. Three-dimensional perspective of the borehole configuration for the Drift Scale Test (DST).

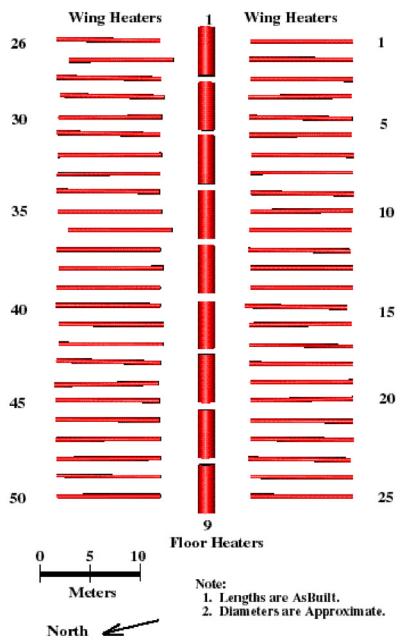

Figure 8. Plan view of the heated drift, nine canister heaters and 50 wing heaters of the DST.

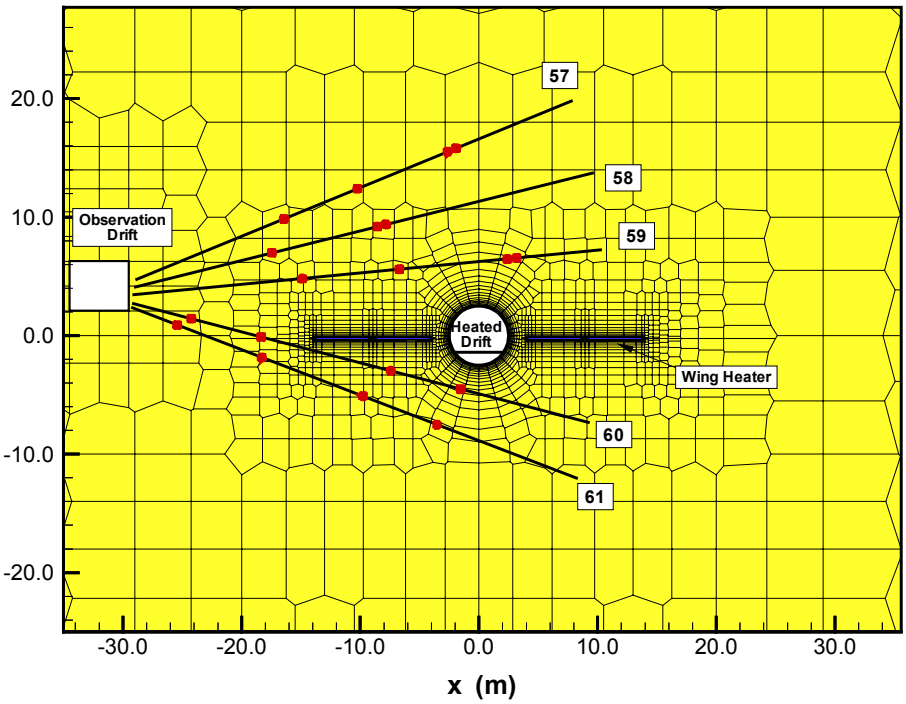

Figure 9. Close-up 2-D vertical section intersecting five hydrology holes 57 through 61.

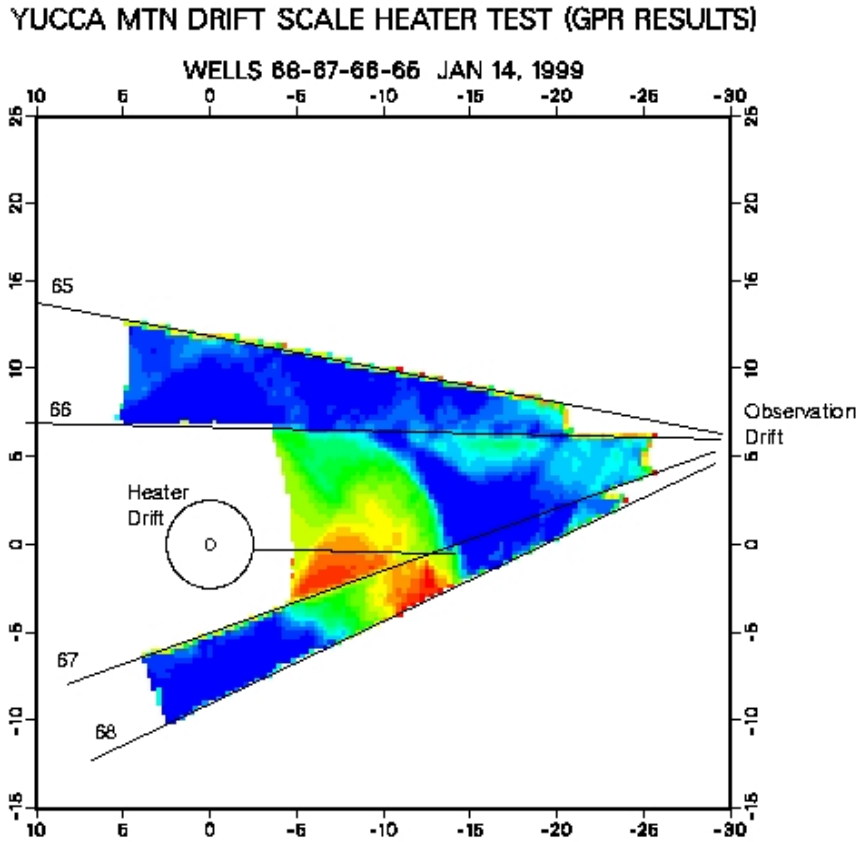

Figure 10. Tomogram of liquid saturation changes from cross-hole radar survey in a vertical x-z section containing boreholes 65 through 68 at 13 months of heating. Red indicates decrease in saturation over time.

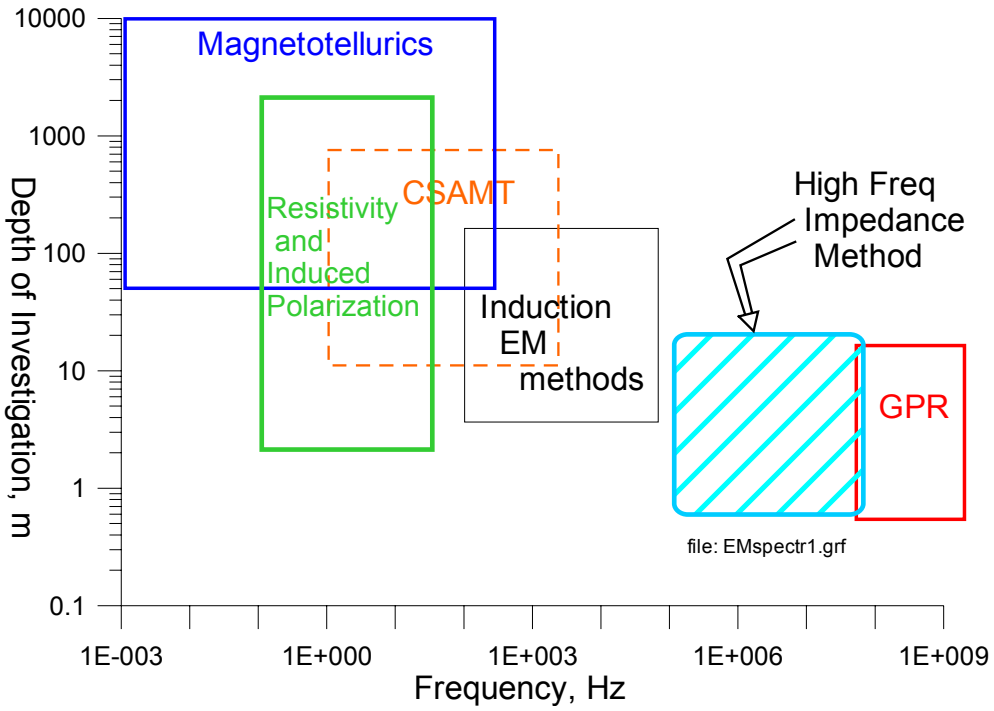

Figure 11. Ranges of applicability of electrical geophysical methods.

Air, grass, and vegetation		
Top soil	$\varepsilon_1 = 10$	0.61 m
Gravel	$\varepsilon_2 = 5$	0.23 m
Clay	$\varepsilon_3 =$ var.	0.61 m
Soil	$\varepsilon_4 = 10$	

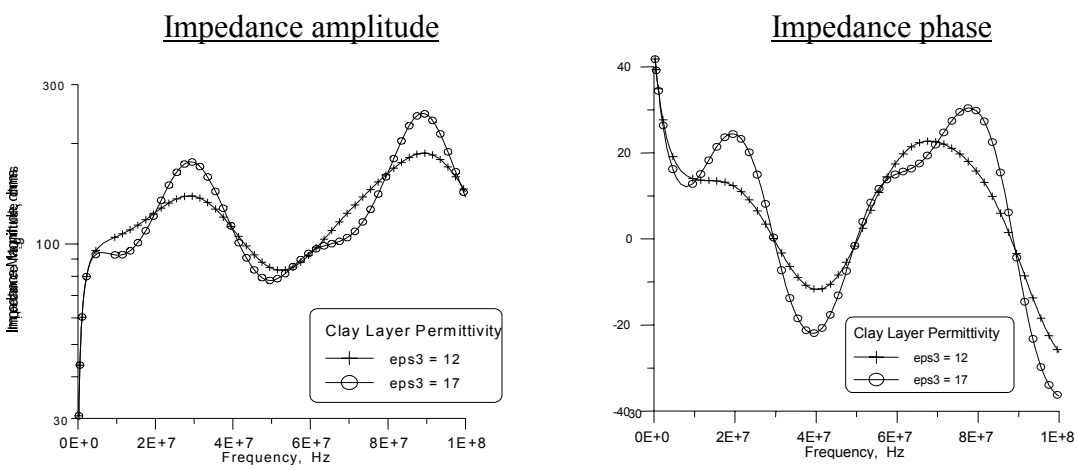

Figure 12. Clay cap model and electromagnetic impedance response on it.

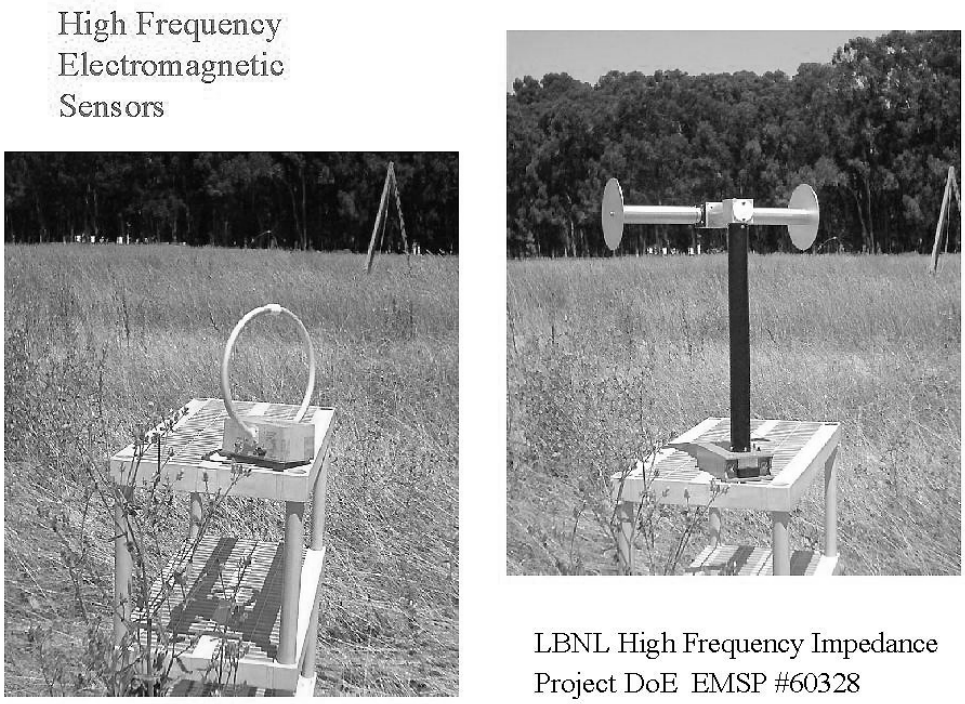

Figure 13. HFI system components. (A) loop magnetic sensor, and (B) stub electric field antenna.

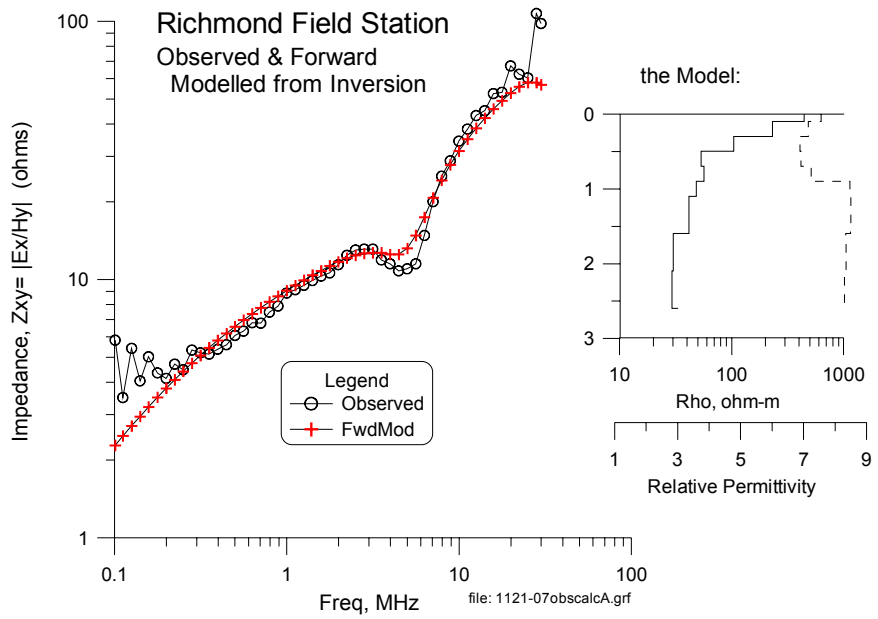

Figure 14. Data obtained at the Richmond Field Station and fitting with 1-D inversion (on the right). Horizontal magnetic dipole (My) was used as source. Inversion was done using Occam's algorithm.

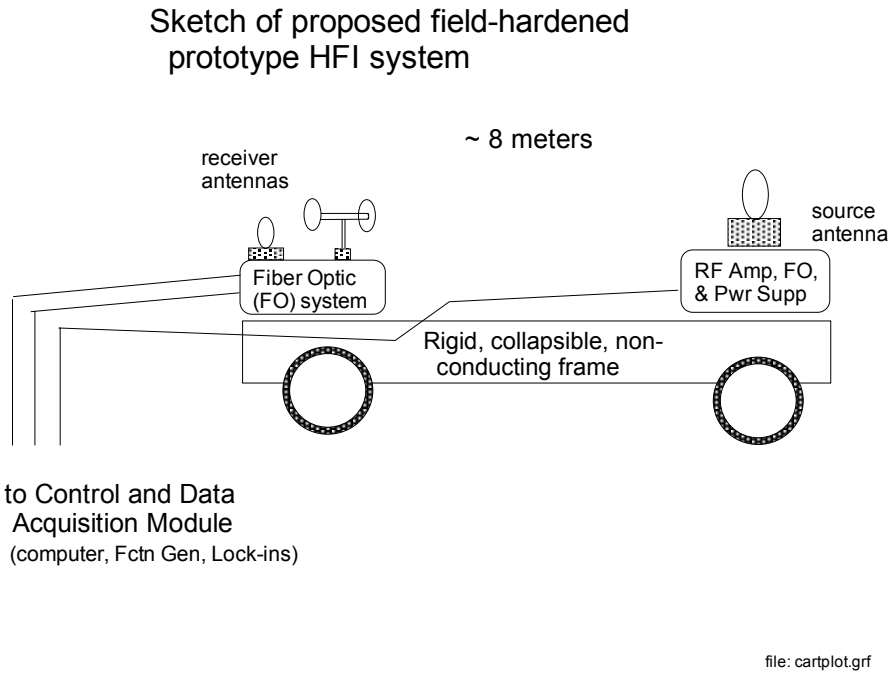

Figure 15. A computer-controlled, optical fiber connected prototype HFI system.